

# Text Embedding Knows How to Quantize Text-Guided Diffusion Models

Hongjae Lee    Myungjun Son    Dongjea Kang    Seung-Won Jung \*

Korea University

{jimmy9704, sonbill, kedjk11, swjung83}@korea.ac.kr

## Abstract

*Despite the success of diffusion models in image generation tasks such as text-to-image, the enormous computational complexity of diffusion models limits their use in resource-constrained environments. To address this, network quantization has emerged as a promising solution for designing efficient diffusion models. However, existing diffusion model quantization methods do not consider input conditions, such as text prompts, as an essential source of information for quantization. In this paper, we propose a novel quantization method dubbed Quantization of Language-to-Image diffusion models using text Prompts (QLIP). QLIP leverages text prompts to guide the selection of bit precision for every layer at each time step. In addition, QLIP can be seamlessly integrated into existing quantization methods to enhance quantization efficiency. Our extensive experiments demonstrate the effectiveness of QLIP in reducing computational complexity and improving the quality of the generated images across various datasets. The source code is available at our project page <https://github.com/jimmy9704/QLIP>.*

## 1. Introduction

Diffusion models have achieved remarkable success in various generative tasks, particularly in text-to-image generation [42, 43, 62]. However, the huge computational complexity of diffusion models restricts their practical applicability, especially in resource-constrained environments. Specifically, diffusion models typically require hundreds of denoising steps to produce high-quality samples, making them considerably slower than generative adversarial networks (GANs) [12]. To this end, many studies introduced advanced training-free samplers to reduce the number of denoising iterations [4, 32, 34, 51]. However, the decrease in iterations alone is insufficient since the denoising models used in each iteration possess billions of parameters [6, 40, 45], leading to increased computational com-

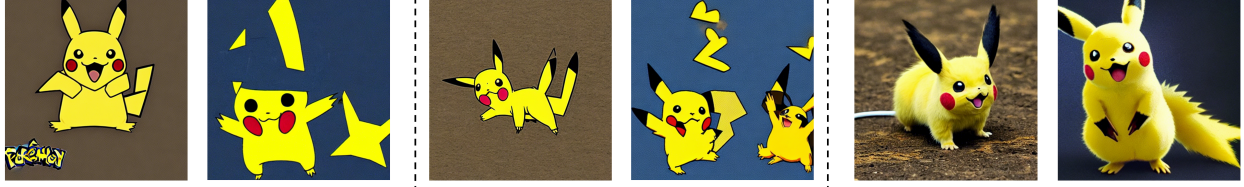
plexity and high memory consumption.

Besides other approaches toward light-weight network designs, such as network architecture search [10, 31], network pruning [14, 53], and knowledge distillation [26, 61], network quantization has received particular attention due to its simplicity, the increasing demand for low-precision operations, and related hardware support [11, 59, 63]. Although various network quantization methods have been proposed for convolutional neural networks (CNNs), the direct use of such methods for diffusion models has shown significant performance degradation [48]. As tailored solutions for diffusion models, several methods have been proposed considering the time step of diffusion models for quantization. For example, PTQ4DM [48] performed 8-bit quantization by constructing a calibration dataset based on the time step. Q-Diffusion [27] introduced an advanced method based on BRECQ [28] and performed the performance analysis of quantization methods for text-guided diffusion models. In addition, TDQ [50] performed quantization with varying activation scaling based on the diffusion time step. However, these methods do not use the text prompt provided to the diffusion model as valuable information for quantization, leaving room for further improvement.

Meanwhile, recent studies highlight the advantages of dynamic bit precision quantization considering input conditions [33, 56]. For example, in the case of image super-resolution, CADyQ [20] and AdaBM [19] performed dynamic quantization according to the complexity of the images and the importance of layers. RefQSR [25] clustered the image patches and assigned high-bit and low-bit precisions to the reference and query patches, respectively. These dynamic quantization methods allow for the cost-effective assignment of bit precision, enhancing quantization efficiency. However, such input-adaptive quantization methods have not yet been explored in diffusion models.

In this paper, we propose a novel quantization method, dubbed Quantization of Language-to-Image diffusion models using text Prompts (QLIP), which determines the bit precision of diffusion models according to the text prompt. Figure 1 shows our observation: The quality of the gener-

\*corresponding author



Pikachu, the symbol and eternal mascot of Pokémon, is the most famous of over 1,000 Pokémon and is a Pokémon with an electric attribute. It appeared in various video games, TV shows, movies, and merchandise since its introduction in the late 1990s.

Pikachu

Pikachu is a small, yellow, mouse-like creature with large, black-tipped ears that resemble lightning bolts. It has rosy cheeks, a small mouth, and large, expressive eyes. Pikachu's body is covered in soft, yellow fur, and it has a long, lightning bolt-shaped tail.

Figure 1. Examples of the images generated by Stable Diffusion v1.4 using the text prompts given below images. When the text prompt details the shape, texture, and properties for the target object, the generated images have rich details and textures, as shown on the right; whereas the generated images are not very different from the images generated using only the keyword when the text prompt is less specific to the target object, as shown on the left.

ated images increases as the text prompt has more specific information about the image to be generated. This suggests that high-bit precision operations are necessary to generate images with vivid details and textures corresponding to detailed text prompts; whereas, low-bit precision operations can be sufficient to generate images corresponding to text prompts that lack specific guidance on details and textures.

Motivated by this observation, we quantized the diffusion model [42] using Q-diffusion [27] with high-bit and low-bit settings and compared the quality of the generated images with the full-precision model. As shown in Figure 2, the performance drop of the low-bit model is noticeable when the quality of the generated images is high for the full-precision model. In contrast, when the quality is low for the full-precision model, the high-bit and low-bit models perform similarly to the full-precision model. These results suggest that diffusion models can be efficiently quantized without sacrificing performance if the quality of the generated images can be first predicted and then used to determine bit precision. Accordingly, our proposed QLIP predicts the image quality from the text prompt and determines the quantization bit precision for diffusion models.

Furthermore, previous studies [15, 27, 48, 50] revealed that the activation distributions of diffusion models vary across layers over time steps. Inspired by these studies, QLIP uses learnable parameters to determine the bit precision for each layer and for each timestep. Our contributions can be summarized as follows:

- To the best of our knowledge, QLIP is the first approach that explicitly utilizes text prompts for dynamic quantization in diffusion models.
- We propose leveraging text prompts to predict the image quality, which is used to guide the selection of bit precision for every layer in different denoising time steps.
- Our proposed QLIP can be integrated into existing diffusion quantization methods to enhance quantization efficiency.

## 2. Related work

### 2.1. Computationally efficient diffusion models

Diffusion models generate high-quality images by iteratively removing noise from random noise. Despite their capability to generate high-quality images, diffusion models encounter challenges in real-world applications due to the time-consuming iterative denoising process. Thus, many efforts have been made to make the diffusion process computationally efficient, including reducing the number of iterative diffusion processes via a non-Markovian process [51], adjusting the variance scheduling [36], and employing knowledge distillation [35, 46].

Meanwhile, since the computational complexity of diffusion model architectures also limits their practical applicability, especially in resource-constrained environments, research efforts have been made to lighten denoising models. For example, SnapFusion [29] introduced an efficient U-Net architecture based on Stable Diffusion [42], while BKSDM [21] further lightened the architecture through knowledge distillation.

### 2.2. Quantization of diffusion models

Quantization involves mapping 32-bit floating-point values of weights and activations to lower-bit values. Numerous studies have explored quantization to compress and accelerate neural networks [7, 20], which can be classified into two approaches: quantization-aware training (QAT) and post-training quantization (PTQ). Recent studies [9, 38, 44, 55] on quantizing diffusion models have focused mainly on PTQ due to the inability to use training data for privacy and commercial reasons, as well as the high computational cost of QAT. Specifically, PTQ4DM [48] and Q-diffusion [27] performed quantization of diffusion models by generating a time step-aware calibration set that consists of data sampled across various time steps using the full-precision denoising model. PTQD [15] separated the



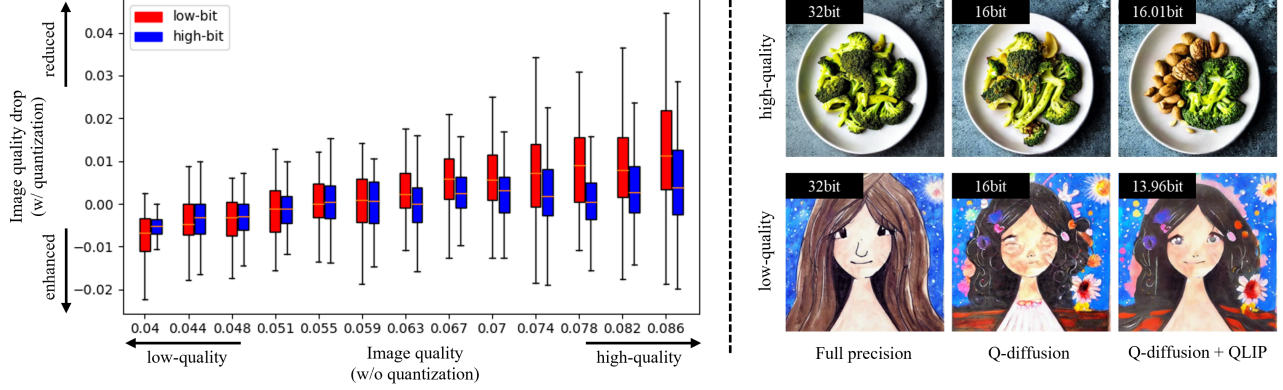


Figure 2. Analysis of the effect of quantization and the quality of generated images, where the image quality is measured using the GIQA score [13]. On the left side, the x-axis represents the quality of images generated by the full-precision model, and the y-axis represents the quality difference between the generated images using the full-precision and quantized models. The images are generated by Stable Diffusion v1.4 [42] using 5000 captions from the COCO 2017 dataset [30] with a size of  $512 \times 512$ . The high-bit (W4A10) and low-bit (W4A6) quantized models are obtained by applying Q-diffusion [27]. On the right side, examples of images generated using models that are unquantized or quantized w/o QLIP are shown for two different image quality levels.

quantization noise from the diffusion noise to reduce quantization errors. Additionally, PTQD introduced a time step-based mixed-precision method but did not employ varying bit precision for each layer. Furthermore, TDQ [50] performed quantization by adaptively scaling the activations for different diffusion time steps and layers, but assigned the same bit precision for all time steps. Although these diffusion model quantization methods have shown progress in reducing the complexity of noise estimation models, they do not adjust quantization parameters based on input conditions such as text prompts.

### 2.3. Input-adaptive dynamic quantization

Recent advances in hardware have enabled mixed-precision operations, allowing various layers to use different bit precisions to improve performance and computational efficiency [11, 59]. Many methods have been proposed to determine the bit precision of each layer of CNNs [11, 33, 59]. For example, several input-adaptive dynamic quantization methods [19, 20, 25, 56] have been introduced for super-resolution, which adjust bit precisions based on the complexity of image patches and the sensitivity to quantization. However, diffusion models have not yet explored such input-adaptive quantization methods. Therefore, this paper proposes a novel quantization method for text-guided diffusion models that applies adaptive quantization using input conditions.

## 3. Method

### 3.1. Preliminaries

**Diffusion model.** The reverse process of a diffusion model gradually removes noise from random data  $\mathbf{x}_t$  to

produce a high-quality image  $\mathbf{x}_0$ , which can be expressed as  $p_\theta(\mathbf{x}_{t-1}|\mathbf{x}_t) = \mathcal{N}(\mathbf{x}_{t-1}; \mu_\theta(\mathbf{x}_t, t), \sigma_t^2 \mathbf{I})$ . The denoising process at time step  $t$  using the noise estimation model  $\epsilon_\theta$  can then be represented as follows:

$$\mu_\theta(\mathbf{x}_t, t) = \frac{1}{\sqrt{\alpha_t}} \left( \mathbf{x}_t - \frac{\beta_t}{\sqrt{1 - \bar{\alpha}_t}} \epsilon_\theta(\mathbf{x}_t, t) \right), \quad (1)$$

where  $\alpha_t$ ,  $\bar{\alpha}_t$ , and  $\beta_t$  are the parameters that control the strength of the Gaussian noise in each step, and  $\sigma_t$  is a variance schedule [18].

**Diffusion model quantization.** Diffusion model quantization reduces the complexity of a noise estimation model that requires hundreds of iterative sampling processes. The denoising process at time step  $t$  using the quantized noise estimation model  $\hat{\epsilon}_\theta$  and the quantized data  $\hat{\mathbf{x}}_t$  can be expressed as follows:

$$\hat{\mu}_\theta(\hat{\mathbf{x}}_t, t) = \frac{1}{\sqrt{\alpha_t}} \left( \hat{\mathbf{x}}_t - \frac{\beta_t}{\sqrt{1 - \bar{\alpha}_t}} \hat{\epsilon}_\theta(\hat{\mathbf{x}}_t, t) \right), \quad (2)$$

where  $\hat{\epsilon}_\theta = Q_{\mathbf{b}^t}(\epsilon_\theta)$ .

Here,  $\mathbf{b}^t \in \mathbb{R}^K$  represents a set of quantization bit precisions for  $K$  layers at time step  $t$ , and  $Q_{\mathbf{b}^t}$  is a function that performs layer-wise and time step-wise quantization using  $\mathbf{b}^t$ . To our knowledge, all previous diffusion quantization methods set the same bit precision to all layers, *i.e.*,  $\mathbf{b}^t(1) = \mathbf{b}^t(2) = \dots = \mathbf{b}^t(K)$ , and only a few methods [15, 55] performed time step-wise dynamic quantization, *i.e.*,  $\mathbf{b}^{t_i} \neq \mathbf{b}^{t_j}$  for some time steps  $t_i$  and  $t_j$ ,  $t_i \neq t_j$ . However, such methods do not adapt the bit precision for each layer. Our proposed QLIP determines  $\mathbf{b}^t$  by training so that the quantization error can be effectively reduced without sacrificing the performance of diffusion models.

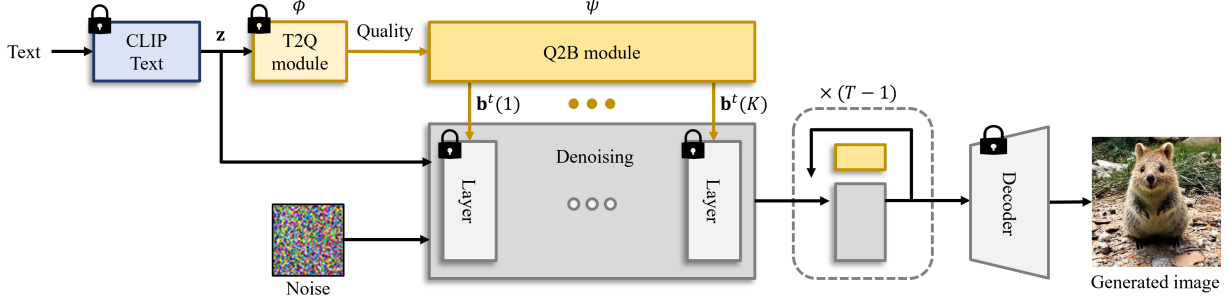


Figure 3. Overview of QLIP that consists of two key modules: T2Q module that predicts image quality from the input text prompt and Q2B module that determines bit precisions for all denoising layers and time steps. Only the Q2B module is trained during QLIP training. See Sections 3.3 and 3.4 for the details about the pre-training of the T2Q module and diffusion models.

### 3.2. Framework overview

Our observations shown in Figure 2 indicate that bit precisions for quantization can be determined cost-effectively given the quality of the generated image. However, this image quality remains unknown during the inference stage, motivating us to predict it using an available input, *i.e.*, text prompts. Specifically, if text prompts have rich and detailed information, the expected quality of the generated image is high, and vice versa. To this end, we introduce a text-to-quality (T2Q) module  $\phi$  that predicts image quality  $q$  from the embedding vector  $\mathbf{z}$ , *i.e.*,  $q = \phi(\mathbf{z})$ , where  $\mathbf{z}$  is obtained by CLIP-Text [41] using the input text prompt.

Next, as we discussed, high-bit quantization is required to generate images with vivid details and textures corresponding to detailed text prompts; while low-bit quantization is sufficient to generate images using less specific text prompts. Therefore, we design a quality-to-bit (Q2B) module  $\psi$  that maps image quality  $q$  to appropriate bit precision, *i.e.*,  $\mathbf{b}^t = \psi(q)$ . Note that the Q2B module determines bit precisions for each time step for different layers since the activation distributions of diffusion models vary across layers over time steps.

In summary, the proposed QLIP obtains a quantized diffusion model  $\hat{\epsilon}_\theta = Q_{\psi(\phi(\mathbf{z}))}(\epsilon_\theta)$  by learning the parameters of  $\psi$  and  $\phi$ . The overview of the proposed QLIP is shown in Figure 3. The following subsections detail the T2Q and Q2B modules and their training procedure and loss functions.

### 3.3. Text-to-Quality estimation

The T2Q module, denoted as  $\phi$ , aims to predict the image quality from the input text prompt.  $\phi$  consists of three linear layers and outputs an image quality score  $q$  as  $q = \phi(\mathbf{z})$ , where  $\mathbf{z} \in \mathbb{R}^{C_{clip}}$  represents the CLIP text embedding, and  $C_{clip}$  denotes its channel dimension. For the training of the T2Q module, we collect a dataset  $\mathcal{T}_{T2Q} = \{\mathbf{z}^i, \mathbf{x}_0^i\}_{i=1}^{N_{T2Q}}$ , where  $\mathbf{z}^i$  and  $\mathbf{x}_0^i$  are the  $i$ -th sample of the CLIP text embedding and its corresponding generated

image obtained using the full-precision diffusion model, respectively, and  $N_{T2Q}$  is the number of images in  $\mathcal{T}_{T2Q}$ . Let  $\bar{q}^i$  represent the (pseudo) ground-truth image quality of  $\mathbf{x}_0^i$ , where we used GIQA [13] as the default quality measure, with an additional normalization to make the range of quality values  $[0, 1]$ . See Section 4.4 for the performance analysis with different quality measures. The T2Q module is trained using the loss  $L_{t2q}$ :

$$L_{t2q} = \frac{1}{N_{T2Q}} \sum_{i=1}^{N_{T2Q}} (\bar{q}^i - \phi(\mathbf{z}^i))^2. \quad (3)$$

Once the T2Q module is trained, it is frozen during the training of the Q2B module and served as a quality predictor to help determine quantization bit precisions.

### 3.4. Quality-to-Bit estimation

In text-guided diffusion models, the richer and more detailed the information in the text prompt is, the higher the image quality tends to be, requiring the use of higher bits. Therefore, the image quality  $q$  predicted by the T2Q module can serve as a direct hint for bit selection. To this end, the proposed Q2B module obtains a probability vector  $\mathbf{p}_q \in \mathbb{R}^K$  for bit selection as follows:

$$\mathbf{p}_q = \sigma((q - 0.5)\mathbf{s} + \mathbf{o}), \quad (4)$$

where  $\mathbf{s} \in \mathbb{R}^K$  and  $\mathbf{o} \in \mathbb{R}^K$  represent sets of learnable parameters, and  $\sigma$  denotes the sigmoid function. Furthermore, to adjust the bit precision for each time step, additional learnable parameters  $\mathbf{u}_m^t \in \mathbb{R}^K$  and  $\mathbf{u}_h^t \in \mathbb{R}^K$  are introduced to obtain probability vectors  $\mathbf{p}_m^t \in \mathbb{R}^K$  and  $\mathbf{p}_h^t \in \mathbb{R}^K$  as

$$\mathbf{p}_j^t = \sigma(\mathbf{u}_j^t), \quad j \in \{m, h\}, t = 1, 2, \dots, T, \quad (5)$$

where  $T$  is the total number of denoising time steps.

These probability vectors,  $\mathbf{p}_q$ ,  $\mathbf{p}_m^t$ , and  $\mathbf{p}_h^t$ , are used to determine the bit precision for each layer and each time

step. Specifically, we define a set of supported bit precisions as  $\mathcal{B} = \{b_{low}, b_{med}, b_{high}\}$ . Then, the probabilities of selecting  $b_{low}$ ,  $b_{med}$ , and  $b_{high}$  are obtained as

$$\begin{aligned} \mathbf{p}_{b_{low}}^t &= (1 - \mathbf{p}_q) \odot (1 - \mathbf{p}_m^t), \\ \mathbf{p}_{b_{med}}^t &= (1 - \mathbf{p}_q) \odot \mathbf{p}_m^t + \mathbf{p}_q \odot (1 - \mathbf{p}_h^t), \\ \mathbf{p}_{b_{high}}^t &= \mathbf{p}_q \odot \mathbf{p}_h^t, \end{aligned} \quad (6)$$

where  $\odot$  represents element-wise multiplication,  $\mathbf{p}_{b_{low}}^t \in \mathbb{R}^K$ ,  $\mathbf{p}_{b_{med}}^t \in \mathbb{R}^K$ , and  $\mathbf{p}_{b_{high}}^t \in \mathbb{R}^K$  are the probability vectors for bit selection. Finally, the bit precision for each layer at time step  $t$  is determined as follows:

$$\mathbf{b}^t(k) = \underset{i \in \{b_{low}, b_{med}, b_{high}\}}{\operatorname{argmax}} \quad \mathbf{p}_i^t(k), \quad k = 1, 2, \dots, K. \quad (7)$$

However, the training of  $\mathbf{u}_m^t$  and  $\mathbf{u}_h^t$  for all  $t$  poses a challenge as  $T$  increases. In addition, the activation distributions of the diffusion models are known to be similar to each other for adjacent time steps [15, 50]. Consequently, we learn the parameters for every  $M$  time step, *i.e.*,  $\mathbf{u}_j^{Mt}$ , and use the same parameters for the intermediate time steps, *i.e.*,  $\mathbf{u}_j^{M(t+1)-1} = \mathbf{u}_j^{M(t+1)-2} = \dots = \mathbf{u}_j^{Mt}$ ,  $j \in \{m, h\}$ . Next, previous studies [3, 8] revealed that the initial stage of the reverse process involves generating the rough context of an image corresponding to the input text prompt; thus, the use of low bits in the initial time steps could decrease the correlation between the text prompt and the generated image. Therefore, we set all values in  $\mathbf{p}_q$  to 1 for the first  $m$  time steps in Equation (6) to enforce the selection of high bits in the initial stage of the reverse process. In summary, the Q2B module has  $2K$  ( $\mathbf{s}$  and  $\mathbf{o}$ ) +  $2KT/M$  ( $\mathbf{u}_m^t$  and  $\mathbf{u}_h^t$ ) trainable parameters.

The bit selection in Equation (7) is non-differentiable, making it unable to backpropagate. Thus, we adopt a straight-through estimator [5] to render this process differentiable:

$$\begin{aligned} \hat{\mathbf{a}}^t(k) &= \\ \begin{cases} Q_{\mathbf{b}^t(k)}(\mathbf{a}^t(k)) & \text{forward,} \\ \sum_{i \in \{b_{low}, b_{med}, b_{high}\}} \mathbf{p}_i^t(k) \cdot Q_i(\mathbf{a}^t(k)) & \text{backward.} \end{cases} \end{aligned} \quad (8)$$

Here,  $\mathbf{a}^t(k)$  and  $\hat{\mathbf{a}}^t(k)$  represent the activations of the full-precision and quantized models at time step  $t$  of the  $k$ -th layer. In other words, during backpropagation, the activations quantized by all bit precisions in  $\mathcal{B}$  are weighted by their corresponding estimated probabilities. Since diffusion models are less sensitive to the quantization of the weights [15, 27], the weights are quantized using a fixed precision, which is empirically chosen as 4 bits for all layers and time steps.

Given the full precision diffusion model, we obtain its quantized weights by applying the baseline diffusion quantization methods [15, 27]. The quantization parameters, including the maximum and minimum values for clipping, are

also predetermined for all bit precisions in  $\mathcal{B}$ . Then, while freezing all the other modules in Figure 3, only the Q2B module is trained using a small calibration set. The Q2B module is trained at randomly sampled time steps  $t$  using the loss function  $L_{QLIP}$ :

$$\begin{aligned} L_{QLIP} &= (\epsilon_\theta(\mathbf{x}_t, t) - \hat{\epsilon}_\theta(\hat{\mathbf{x}}_t, t))^2 \\ &+ \lambda_{bit} \left( b_{high} \cdot \sum_{k=1}^K \mathbf{p}_{b_{high}}^t(k) + b_{med} \cdot \sum_{k=1}^K \mathbf{p}_{b_{med}}^t(k) \right). \end{aligned} \quad (9)$$

Here, the first term measures the difference between the results of the full-precision and quantized models, and the second term measures the bit lengths for the high- and medium-precision models.  $\lambda_{bit}$  is a weighting parameter that balances between these two terms.

## 4. Experiments

### 4.1. Experimental setup

**Datasets and baseline quantization methods.** To evaluate the effectiveness of QLIP across different diffusion models, we conducted experiments using two diffusion networks: BK-SDM-Tiny-2M [21] and Stable Diffusion v1.4 [42]. Our experiments involve two datasets, COCO2017 [30] and Conceptual Captions [49]. To train the T2Q module, 10k images were generated by Stable Diffusion v1.4 [42] using 10k text annotations in the COCO2017 training dataset as input text prompts. We generated another 1024 images using unused text annotations in the COCO2017 training dataset to train the Q2B module. We evaluated the effectiveness of our proposed QLIP by applying it to the baseline diffusion quantization methods, Q-diffusion [27] and PTQD [15]. In the implementation of PTQD, we set the noise correction parameter to  $b_{med}$ , while noise correction was not applied if the estimated image quality by the T2Q module is below 0.3 or above 0.7. We trained the T2Q module for 3 epochs using the Adam optimizer [22] with a learning rate of 0.001 and the Q2B module for 5000 iterations using BRECQ [28], as adopted in Q-diffusion and PTQD, using RTX 3090. For performance evaluation, following the baseline quantization method [27], we generated 10k images using 10k text annotations in the COCO2017 validation dataset. Moreover, to evaluate the generalization ability of the quantized models, we used Conceptual Captions to generate additional 10k images.

**Evaluation metrics.** We report widely adopted metrics such as FID [17] and sFID [47] to evaluate image quality. In addition, we use CLIP Score [16] to assess the degree of matching between the generated images and their corresponding text prompts. To quantify computational efficiency, we measure BitOPs [25, 57], which account for the



COCO2017						
Method	Bitoptions	FAB $\downarrow$	BitOPs (T) $\downarrow$	FID $\downarrow$	sFID $\downarrow$	CLIP Score $\uparrow$
BK-SDM [21]	W32A32	32.00	10.46	23.79	66.19	0.3069
Q-diffusion [27]	W4A16	16.00	1.03	30.02	73.25	<b>0.3068</b>
+QLIP	W4A{8,16,32}	<b>12.14</b>	<b>0.88</b>	<b>30.01</b>	<b>73.24</b>	0.3063
PTQD [15]	W4A16	16.00	1.03	30.27	77.18	<b>0.3069</b>
+QLIP	W4A{8,16,32}	<b>12.14</b>	<b>0.88</b>	<b>30.02</b>	<b>73.26</b>	0.3063
Conceptual Captions						
Method	Bitoptions	FAB $\downarrow$	BitOPs (T) $\downarrow$	FID $\downarrow$	sFID $\downarrow$	CLIP Score $\uparrow$
BK-SDM [21]	W32A32	32.00	10.46	20.00	47.80	0.2983
Q-diffusion [27]	W4A16	16.00	1.03	<b>24.68</b>	62.70	<b>0.2965</b>
+QLIP	W4A{8,16,32}	<b>10.58</b>	<b>0.82</b>	24.72	<b>59.54</b>	0.2964
PTQD [15]	W4A16	16.00	1.03	<b>24.66</b>	62.60	0.2965
+QLIP	W4A{8,16,32}	<b>10.58</b>	<b>0.82</b>	24.71	<b>59.25</b>	<b>0.2966</b>

Table 1. Quantitative comparisons of various quantization methods at a resolution of  $512 \times 512$  using BK-SDM-Tiny-2M.

COCO2017					
Method	FAB $\downarrow$	FID $\downarrow$	sFID $\downarrow$	CLIP Score $\uparrow$	
Stable Diffusion [42]	32.00	22.23	65.11	0.3174	
Q-diffusion [27]	8.00	23.40	66.57	<b>0.3126</b>	
+QLIP	<b>7.86</b>	<b>21.61</b>	<b>64.32</b>	0.3120	
PTQD [15]	8.00	22.75	68.63	<b>0.3126</b>	
+QLIP	<b>7.86</b>	<b>21.35</b>	<b>65.81</b>	0.3120	
Conceptual Captions					
Method	FAB $\downarrow$	FID $\downarrow$	sFID $\downarrow$	CLIP Score $\uparrow$	
Stable Diffusion [42]	32.00	15.67	45.61	0.3078	
Q-diffusion [27]	8.00	20.74	48.33	<b>0.2984</b>	
+QLIP	<b>7.77</b>	<b>19.89</b>	<b>47.63</b>	0.2979	
PTQD [15]	8.00	25.40	55.01	0.2972	
+QLIP	<b>7.77</b>	<b>20.42</b>	<b>48.83</b>	<b>0.2975</b>	

Table 2. Quantitative comparisons of various quantization methods at a resolution of  $512 \times 512$  using Stable Diffusion v1.4. For the bit precision options, W4A8 is used for Q-diffusion and PTQD, and W4A{6,8,10} are used for QLIP.

required operations in both the denoising model and additional modules for QLIP implementation, and feature average bit-width (FAB) [19, 20] for the denoising model. In particular, BitOPs are measured as  $MACs \cdot \frac{b_w}{32} \cdot \frac{b_a}{32}$ , where  $MACs$  denotes multiply-accumulate computations, and  $b_w$  and  $b_a$  represent the bitwidths of weights and activations, respectively.

**Hyperparameter settings.** We conducted experiments on various hyperparameter settings for the COCO2017 validation dataset using Q-diffusion as the baseline in Stable Diffusion v1.4. First, Figure 4(a) presents the results obtained with various values of the weight term  $\lambda_{bit}$  in Equation (9), where  $\lambda_{bit} = 1$  showed an effective balance between FID and FAB. Next, Figure 4(b) shows the results for different

Method	Bitoptions	Runtime (s) $\downarrow$	FAB $\downarrow$	FID $\downarrow$
BK-SDM [21]	W32A32	6.50	32.00	20.00
Q-diffusion [27]	W4A8	<b>4.53</b>	<b>8.00</b>	28.32
Q-diffusion [27]	W4A16	5.58	16.00	<b>24.68</b>
+QLIP	W4A{8,16,32}	4.85	10.58	24.72

Table 3. Runtime comparisons, where W4A{8,16,32} is used for QLIP. Measured on the Conceptual Captions dataset.

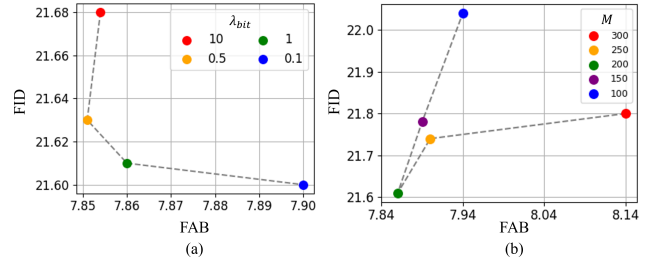


Figure 4. Results on Q-diffusion using different hyperparameter settings of QLIP (W4A{6,8,10}): (a)  $\lambda_{bit}$  and (b)  $M$ .

$M$  values in  $\mathbf{u}_j^{Mt}, j \in \{m, h\}$  when the maximum timestep  $T$  was 1000, where we obtained the best scores with  $M = 200$ .

## 4.2. Quantitative results

**Comparison with existing quantization methods.** To demonstrate the effectiveness and applicability of QLIP, we tested QLIP on two diffusion model quantization methods: Q-diffusion [27] and PTQD [15]. Tables 1 and 2 provides comparison results for the COCO2017 [30] and Conceptual Captions [49] datasets using lightweight diffusion model BK-SDM-Tiny-2M [21] and Stable Diffusion v1.4 [42], respectively.

As shown in Table 1, for the COCO2017 dataset, QLIP





Images	Richness controlled captions	FAB	Images	Richness controlled captions	FAB
	night sky	14.21		retro camera	13.98
	night sky is a vast.	14.99		retro camera has a square frame with metal body and leather grip.	14.10
	night sky is a vast, filled with twinkling stars.	15.16		retro camera has a boxy metal body, leather accents, and a large lens.	14.40
	night sky is a vast, celestial expanse filled with twinkling stars.	15.80		retro camera has a metal frame, leather casing, and a large, rounded glass lens with delicate dials.	15.15
	night sky is a vast, celestial expanse filled with twinkling stars, glowing planets, and the luminous band of the milky way.	16.00		retro camera has a classic metal body, leather wrapping, and a large glass lens, complete with dials and knobs for a timeless, vintage feel.	15.19

Figure 5. Examples of variations in FAB by QLIP for the texts with different levels of richness and detail, along with the generated images.

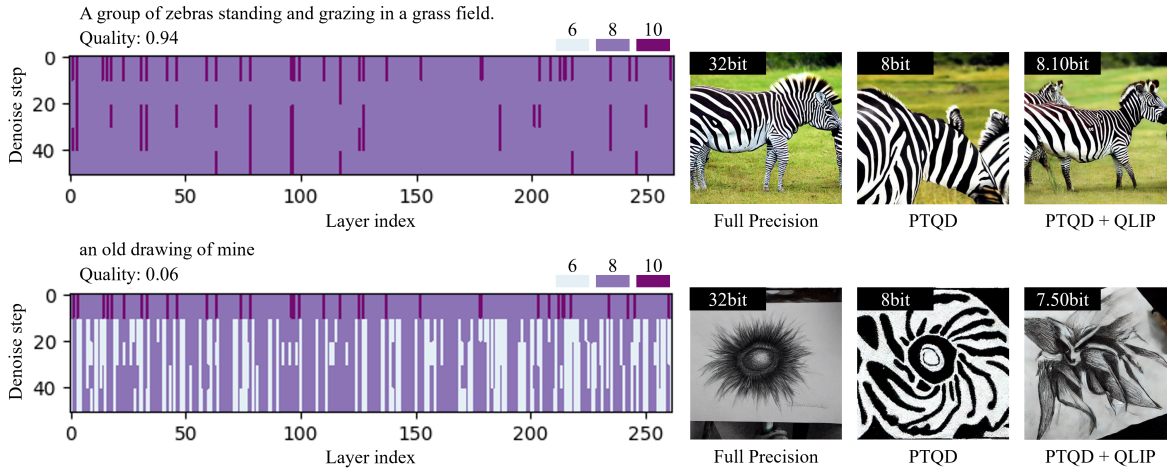


Figure 6. Examples of the bit selection results and generated images. When the text prompt is specifically describing the image to be generated, the predicted image quality is high, and high and medium bits are assigned for most layers and time steps, as shown on the top left. On the other hand, when the text prompt has less detailed information, the predicted image quality is low, and low bits are assigned for many layers and time steps, as shown on the bottom left. On the right side, the generated images using Q-diffusion with and without applying QLIP are shown, demonstrating the effectiveness of QLIP in saving bits while improving the quality of generated images.

effectively reduced computational complexity of the baseline diffusion quantization methods. For example, Q-diffusion+QLIP (W4A{8,16,32}) achieved a reduction in FAB by 3.86 while maintaining similar FID and sFID, compared to Q-diffusion (W4A16). Furthermore, the use of QLIP consistently led to improvements when applied to PTQD, as demonstrated in Table 1. For example, PTQD+QLIP (W4A{8,16,32}) enhanced FID and sFID by 0.25 and 3.92, respectively, while also reducing FAB and BitOPs. The results on Conceptual Captions followed trends similar to those observed in COCO2017. For example, Q-diffusion+QLIP (W4A{8,16,32}) demonstrated reduced computational complexity compared to Q-diffusion on Conceptual Captions.

Table 2 presents the results of applying lower-bit precision combinations to Stable Diffusion v1.4. Here,

PTQD+QLIP (W4A{6,8,10}) achieved a 4.98 improvement in FID compared to PTQD (W4A8), while maintaining similar FAB using bit combinations efficiently. Although our proposed QLIP drives the quantization methods to reduce computational complexity and improve image quality, the CLIP Scores remained similar to those of the baseline quantization methods, indicating that the fitness to the text prompts is not significantly influenced by QLIP. Additional results on larger diffusion models can be found in the supplementary material.

**Runtime measurement.** Runtime was measured with Cutlass [37], including the T2Q and Q2B modules, as shown in Table 3. The results show that runtime was reduced to a level similar to W4A8 while maintaining an FID score comparable to W4A16. Measurements were conducted on an RTX 3090. Additional analysis on memory requirements

can be found in the supplementary material.

### 4.3. Qualitative results

Figure 5 visualizes the changes in FAB by the richness and detail level of the text, along with the generated images. Here, ChatGPT-4o was used to create texts of varying complexity that describe a given keyword. Specifically, the prompt used was “Create four sentences that describe how ‘keyword’ looks like, gradually getting richer and longer.” As can be seen, QLIP assigned higher bits as the text describes the keyword more specifically and in greater detail, demonstrating that it utilizes information from the text to determine bit precisions for effective synthesis of vivid details and textures.

Figure 6 shows several results comparing Q-diffusion with and without QLIP when applied to Stable Diffusion v1.4. As can be seen, our QLIP generates more detailed and natural images compared to PTQD by using various bit combinations. Furthermore, Figure 6 visualizes the bit precision maps determined by QLIP. When the T2Q module predicts high image quality from input text prompts, QLIP allocates more bits to enable rendering of vivid and accurate details from rich text prompts. Otherwise, QLIP employs lower bits for layers that are less sensitive to quantization, based on the text prompt and the time step. For example, when given less specific text prompts, the correlation between the generated image and the text prompt is relatively less critical, allowing for low-bit quantization in the cross-attention blocks. These results highlight the effectiveness and significance of dynamically allocating bit precisions according to text prompts.

### 4.4. Ablation studies

**Ablation studies on the T2Q module.** We report the results on the COCO2017 validation dataset using Stable Diffusion v1.4 with Q-diffusion as the baseline quantization method. Table 4 presents the results of the T2Q modules trained using various perceptual image quality metrics, including Realism score [24], CLIP-IQA [58], and GIQA [13]. The performance of the T2Q module was evaluated using Spearman’s rank-order correlation coefficient (SROCC) [52] and Pearson’s linear correlation coefficient (PLCC) [39] between the actual quality measures and the predictions of the T2Q module. QLIP with GIQA showed the most substantial improvements in FAB and FID along with the highest SROCC and PLCC scores.

**Ablation studies on the Q2B module.** We conducted experiments on several variants of the Q2B module using Q-diffusion and Stable Diffusion v1.4 on the COCO2017 validation dataset. As shown in Table 5, when using either  $\mathbf{p}_q$  alone or in combination with  $\mathbf{p}_h^t$ , effective reduction in FAB was achieved at the expense of increase in FID. When using  $\mathbf{p}_q$  and  $\mathbf{p}_m^t$ , FID decreased while FAB increased. Finally,

Method	SROCC $\uparrow$	PLCC $\uparrow$	FAB $\downarrow$	FID $\downarrow$
Q-diffusion [27]	-	-	8.00	23.40
+QLIP				
w/ Realism score	0.5132	0.5022	8.10	22.18
w/ CLIP-IQA	0.7127	0.7082	8.54	21.81
w/ GIQA	<b>0.8047</b>	<b>0.8108</b>	<b>7.86</b>	<b>21.61</b>

Table 4. Ablation studies on the T2Q module: For the bit precision options, W4A8 in Q-diffusion and +QLIP W4A{6,8,10} were used.

Method	Bitoptions	FAB $\downarrow$	FID $\downarrow$
Q-diffusion [27]	W4A8	8.00	23.40
+ $\mathbf{p}_q$	W4A{6,10}	7.57	26.91
+ $\mathbf{p}_q + \mathbf{p}_h^t$	W4A{6,8,10}	<b>6.73</b>	29.37
+ $\mathbf{p}_q + \mathbf{p}_m^t$	W4A{6,8,10}	8.60	21.96
+ $\mathbf{p}_q + \mathbf{p}_m^t + \mathbf{p}_h^t$ (QLIP)	W4A{6,8,10}	7.86	<b>21.61</b>

Table 5. Ablation studies on the Q2B module.

when  $\mathbf{p}_q$ ,  $\mathbf{p}_h^t$ , and  $\mathbf{p}_m^t$  were all involved, balanced results were obtained in two metrics. Implementation details of the ablation studies on the Q2B module can be found in the supplementary material.

## 5. Conclusion

The proposed quantization method for diffusion models, called QLIP, is the first method that uses text prompts for quantization in diffusion models. From our observation that the bit precision for quantization can be effectively determined based on the quality of the generated images, we designed the T2Q module that predicts image quality from input text prompts. We then introduced the Q2B module that allocates appropriate bit precision for each time step for different layers. By integrating the T2Q and Q2B modules into existing diffusion model quantization methods, we demonstrated the effectiveness of the proposed QLIP. QLIP presents a promising solution for quantizing diffusion models due to its ability to improve the quality of generated images using text prompts while reducing computational costs.

**Limitations and future directions.** Similar to other generative models, QLIP also has the potential to generate counterfeit images for malicious purposes, potentially undermining trust in visual media. In a future study, we will extend QLIP to consider other input conditions, such as images or segmentation maps, in addition to text prompts.

## Acknowledgement

This work was supported by the National Research Foundation of Korea (NRF) grant funded by the Korea government (MSIT) (No. 2022R1A2C2002810).



## References

- [1] FLUX: [huggingface.co/black-forest-labs/flux.1-dev](https://huggingface.co/black-forest-labs/flux.1-dev). 1
- [2] GPT Image 1 API: <https://platform.openai.com/docs/models/gpt-image-1>. 3
- [3] Yogesh Balaji, Seungjun Nah, Xun Huang, Arash Vahdat, Jiaming Song, Qinsheng Zhang, Karsten Kreis, Miika Aittala, Timo Aila, Samuli Laine, et al. eDiff-I: Text-to-image diffusion models with ensemble of expert denoisers. *arXiv preprint arXiv:2211.01324*, 2022. 5
- [4] Fan Bao, Chongxuan Li, Jun Zhu, and Bo Zhang. Analytic-DPM: An analytic estimate of the optimal reverse variance in diffusion probabilistic models. In *Proceedings of the International Conference on Learning Representations*, 2022. 1
- [5] Yoshua Bengio, Nicholas Léonard, and Aaron Courville. Estimating or propagating gradients through stochastic neurons for conditional computation. *arXiv preprint arXiv:1308.3432*, 2013. 5
- [6] James Betker, Gabriel Goh, Li Jing, Tim Brooks, Jianfeng Wang, Linjie Li, Long Ouyang, Juntang Zhuang, Joyce Lee, Yufei Guo, et al. Improving image generation with better captions. *Computer Science*. <https://cdn.openai.com/papers/dall-e-3.pdf>, 2023. 1
- [7] Jungwook Choi, Zhuo Wang, Swagath Venkataramani, Pierce I-Jen Chuang, Vijayalakshmi Srinivasan, and Kailash Gopalakrishnan. PACT: Parameterized clipping activation for quantized neural networks. *arXiv preprint arXiv:1805.06085*, 2018. 2
- [8] Jooyoung Choi, Jungbeom Lee, Chaehun Shin, Sungwon Kim, Hyunwoo Kim, and Sungroh Yoon. Perception prioritized training of diffusion models. In *Proceedings of the IEEE/CVF Conference on Computer Vision and Pattern Recognition*, pages 11472–11481, 2022. 5
- [9] Huanpeng Chu, Wei Wu, Chengjie Zang, and Kun Yuan. QNCD: Quantization noise correction for diffusion models. *arXiv preprint arXiv:2403.19140*, 2024. 2
- [10] Xiangxiang Chu, Shun Lu, Xudong Li, and Bo Zhang. Mix-Path: A unified approach for one-shot neural architecture search. In *Proceedings of the IEEE/CVF International Conference on Computer Vision*, pages 5972–5981, 2023. 1
- [11] Zhen Dong, Zhewei Yao, Amir Gholami, Michael W. Mahoney, and Kurt Keutzer. HAWQ: Hessian aware quantization of neural networks with mixed-precision. In *Proceedings of the IEEE/CVF International Conference on Computer Vision*, pages 293–302, 2019. 1, 3
- [12] Ian Goodfellow, Jean Pouget-Abadie, Mehdi Mirza, Bing Xu, David Warde-Farley, Sherjil Ozair, Aaron Courville, and Yoshua Bengio. Generative adversarial nets. In *Proceedings of the Advances in Neural Information Processing Systems*, pages 2672–2680, 2014. 1
- [13] Shuyang Gu, Jianmin Bao, Dong Chen, and Fang Wen. GIQA: Generated image quality assessment. In *Proceedings of the European Conference on Computer Vision*, pages 369–385, 2020. 3, 4, 8
- [14] Song Han, Jeff Pool, John Tran, and William Dally. Learning both weights and connections for efficient neural network. In *Proceedings of the Advances in Neural Information Processing Systems*, pages 1135–1143, 2015. 1
- [15] Yefei He, Luping Liu, Jing Liu, Weijia Wu, Hong Zhou, and Bohan Zhuang. PTQD: Accurate post-training quantization for diffusion models. In *Proceedings of the Advances in Neural Information Processing Systems*, pages 13237–13249, 2023. 2, 3, 5, 6
- [16] Jack Hessel, Ari Holtzman, Maxwell Forbes, Ronan Le Bras, and Yejin Choi. CLIPScore: A reference-free evaluation metric for image captioning. In *Proceedings of the 2021 Conference on Empirical Methods in Natural Language Processing*, pages 7514–7528, 2021. 5
- [17] Martin Heusel, Hubert Ramsauer, Thomas Unterthiner, Bernhard Nessler, and Sepp Hochreiter. GANs trained by a two time-scale update rule converge to a local nash equilibrium. In *Proceedings of the Advances in Neural Information Processing Systems*, pages 6629–6640, 2017. 5
- [18] Jonathan Ho, Ajay Jain, and Pieter Abbeel. Denoising diffusion probabilistic models. In *Proceedings of the Advances in Neural Information Processing Systems*, pages 6840–6851, 2020. 3
- [19] Cheeun Hong and Kyoung Mu Lee. AdaBM: On-the-fly adaptive bit mapping for image super-resolution. In *Proceedings of the IEEE/CVF Conference on Computer Vision and Pattern Recognition*, pages 2641–2650, 2024. 1, 3, 6
- [20] Cheeun Hong, Sungyong Baik, Heewon Kim, Seungjun Nah, and Kyoung Mu Lee. CADyQ: Content-aware dynamic quantization for image super-resolution. In *Proceedings of the European Conference on Computer Vision*, pages 367–383, 2022. 1, 2, 3, 6
- [21] Bo-Kyeong Kim, Hyoung-Kyu Song, Thibault Castells, and Shinkook Choi. BK-SDM: A lightweight, fast, and cheap version of stable diffusion. In *Proceedings of the European Conference on Computer Vision*, 2024. 2, 5, 6
- [22] Diederik Kingma and Jimmy Ba. Adam: A method for stochastic optimization. In *Proceedings of the International Conference on Learning Representations*, 2015. 5
- [23] Yuval Kirstain, Adam Polyak, Uriel Singer, Shahbuland Matiana, Joe Penna, and Omer Levy. Pick-a-Pic: An open dataset of user preferences for text-to-image generation. In *Proceedings of the Advances in Neural Information Processing Systems Workshop*, 2023. 1
- [24] Tuomas Kynkäänniemi, Tero Karras, Samuli Laine, Jaakko Lehtinen, and Timo Aila. Improved precision and recall metric for assessing generative models. In *Proceedings of the Advances in Neural Information Processing Systems*, pages 3927–3936, 2019. 8
- [25] Hongjae Lee, Jun-Sang Yoo, and Seung-Won Jung. RefQSR: Reference-based quantization for image super-resolution networks. *IEEE Transactions on Image Processing*, 33: 2823–2834, 2024. 1, 3, 5
- [26] Lujun Li, Peijie Dong, Zimian Wei, and Ya Yang. Automated knowledge distillation via monte carlo tree search. In *Proceedings of the IEEE/CVF International Conference on Computer Vision*, pages 17413–17424, 2023. 1
- [27] Xiuyu Li, Yijiang Liu, Long Lian, Huanrui Yang, Zhen Dong, Daniel Kang, Shanghang Zhang, and Kurt Keutzer.

- Q-diffusion: Quantizing diffusion models. In *Proceedings of the IEEE/CVF International Conference on Computer Vision*, pages 17535–17545, 2023. 1, 2, 3, 5, 6, 8
- [28] Yuhang Li, Ruihao Gong, Xu Tan, Yang Yang, Peng Hu, Qi Zhang, Fengwei Yu, Wei Wang, and Shi Gu. BRECC: Pushing the limit of post-training quantization by block reconstruction. In *Proceedings of the International Conference on Learning Representations*, 2021. 1, 5
- [29] Yanyu Li, Huan Wang, Qing Jin, Ju Hu, Pavlo Chemerys, Yun Fu, Yanzhi Wang, Sergey Tulyakov, and Jian Ren. SnapFusion: Text-to-image diffusion model on mobile devices within two seconds. In *Proceedings of the Advances in Neural Information Processing Systems*, pages 20662–20678, 2024. 2
- [30] Tsung-Yi Lin, Michael Maire, Serge Belongie, James Hays, Pietro Perona, Deva Ramanan, Piotr Dollár, and C Lawrence Zitnick. Microsoft COCO: Common objects in context. In *Proceedings of the European Conference on Computer Vision*, pages 740–755, 2014. 3, 5, 6
- [31] Chenxi Liu, Barret Zoph, Maxim Neumann, Jonathon Shlens, Wei Hua, Li-Jia Li, Li Fei-Fei, Alan Yuille, Jonathan Huang, and Kevin Murphy. Progressive neural architecture search. In *Proceedings of the European Conference on Computer Vision*, pages 19–34, 2018. 1
- [32] Luping Liu, Yi Ren, Zhijie Lin, and Zhou Zhao. Pseudo numerical methods for diffusion models on manifolds. In *Proceedings of the International Conference on Learning Representations*, 2022. 1
- [33] Zhenhua Liu, Yunhe Wang, Kai Han, Siwei Ma, and Wen Gao. Instance-aware dynamic neural network quantization. In *Proceedings of the IEEE/CVF Conference on Computer Vision and Pattern Recognition*, pages 12434–12443, 2022. 1, 3
- [34] Cheng Lu, Yuhao Zhou, Fan Bao, Jianfei Chen, Chongxuan Li, and Jun Zhu. DPM-Solver: A fast ODE solver for diffusion probabilistic model sampling in around 10 steps. In *Proceedings of the Advances in Neural Information Processing Systems*, pages 5775–5787, 2022. 1
- [35] Chenlin Meng, Robin Rombach, Ruiqi Gao, Diederik Kingma, Stefano Ermon, Jonathan Ho, and Tim Salimans. On distillation of guided diffusion models. In *Proceedings of the IEEE/CVF Conference on Computer Vision and Pattern Recognition*, pages 14297–14306, 2023. 2
- [36] Alexander Quinn Nichol and Prafulla Dhariwal. Improved denoising diffusion probabilistic models. In *Proceedings of the International Conference on Machine Learning*, pages 8162–8171, 2021. 2
- [37] NVIDIA. CUTLASS, 2025. <https://github.com/NVIDIA/cutlass>. 7
- [38] Nilesh Prasad Pandey, Marios Fournarakis, Chirag Patel, and Markus Nagel. Softmax bias correction for quantized generative models. In *Proceedings of the IEEE/CVF International Conference on Computer Vision Workshop*, pages 1453–1458, 2023. 2
- [39] Karl Pearson. Notes on regression and inheritance in the case of two parents. *Proceedings of the Royal Society of London*, 58:240–242, 1895. 8
- [40] Dustin Podell, Zion English, Kyle Lacey, Andreas Blattmann, Tim Dockhorn, Jonas Müller, Joe Penna, and Robin Rombach. SDXL: Improving latent diffusion models for high-resolution image synthesis. In *Proceedings of the International Conference on Learning Representations*, 2024. 1
- [41] Alec Radford, Jong Wook Kim, Chris Hallacy, Aditya Ramesh, Gabriel Goh, Sandhini Agarwal, Girish Sastry, Amanda Askell, Pamela Mishkin, Jack Clark, et al. Learning transferable visual models from natural language supervision. In *Proceedings of the International Conference on Machine Learning*, pages 8748–8763, 2021. 4
- [42] Robin Rombach, Andreas Blattmann, Dominik Lorenz, Patrick Esser, and Björn Ommer. High-resolution image synthesis with latent diffusion models. In *Proceedings of the IEEE/CVF Conference on Computer Vision and Pattern Recognition*, pages 10674–10685, 2022. 1, 2, 3, 5, 6
- [43] Nataniel Ruiz, Yuanzhen Li, Varun Jampani, Yael Pritch, Michael Rubinstein, and Kfir Aberman. DreamBooth: Fine tuning text-to-image diffusion models for subject-driven generation. In *Proceedings of the IEEE/CVF Conference on Computer Vision and Pattern Recognition*, pages 22500–22510, 2023. 1
- [44] Hyogon Ryu, Seohyun Lim, and Hyunjung Shim. Memory-efficient personalization using quantized diffusion model. In *Proceedings of the European Conference on Computer Vision*, 2024. 2
- [45] Chitwan Saharia, William Chan, Saurabh Saxena, Lala Li, Jay Whang, Emily L Denton, Kamyar Ghasemipour, Raphael Gontijo Lopes, Burcu Karagol Ayan, Tim Salimans, et al. Photorealistic Text-to-Image Diffusion Models with Deep Language Understanding. In *Proceedings of the Advances in Neural Information Processing Systems*, pages 36479–36494, 2022. 1
- [46] Tim Salimans and Jonathan Ho. Progressive distillation for fast sampling of diffusion models. In *Proceedings of the International Conference on Learning Representations*, 2022. 2
- [47] Tim Salimans, Ian Goodfellow, Wojciech Zaremba, Vicki Cheung, Alec Radford, Xi Chen, and Xi Chen. Improved techniques for training gans. In *Proceedings of the Advances in Neural Information Processing Systems*, pages 2234–2242, 2016. 5
- [48] Yuzhang Shang, Zhihang Yuan, Bin Xie, Bingzhe Wu, and Yan Yan. Post-training quantization on diffusion models. In *Proceedings of the IEEE/CVF Conference on Computer Vision and Pattern Recognition*, pages 1972–1981, 2023. 1, 2
- [49] Piyush Sharma, Nan Ding, Sebastian Goodman, and Radu Soricut. Conceptual captions: A cleaned, hypernymed, image alt-text dataset for automatic image captioning. In *Proceedings of the 56th Annual Meeting of the Association for Computational Linguistics*, pages 2556–2565, 2018. 5, 6
- [50] Junhyuk So, Jungwon Lee, Daehyun Ahn, Hyungjun Kim, and Eunhyeok Park. Temporal dynamic quantization for diffusion models. In *Proceedings of the Advances in Neural Information Processing Systems*, pages 48686–48698, 2023. 1, 2, 3, 5

- [51] Jiaming Song, Chenlin Meng, and Stefano Ermon. Denoising diffusion implicit models. In *Proceedings of the International Conference on Learning Representations*, 2021. [1](#), [2](#)
- [52] Charles Spearman. The proof and measurement of association between two things. *The American Journal of Psychology*, 15(1):72—101, 1961. [8](#)
- [53] Yang Sui, Miao Yin, Yi Xie, Huy Phan, Saman Aliari Zonouz, and Bo Yuan. CHIP: Channel independence-based pruning for compact neural networks. In *Proceedings of the Advances in Neural Information Processing Systems*, pages 24604–24616, 2021. [1](#)
- [54] Siao Tang, Xin Wang, Hong Chen, Chaoyu Guan, Zewen Wu, Yansong Tang, and Wenwu Zhu. Post-training quantization with progressive calibration and activation relaxing for text-to-image diffusion models. In *Proceedings of the European Conference on Computer Vision*, pages 404–420, 2024. [1](#)
- [55] Siao Tang, Xin Wang, Hong Chen, Chaoyu Guan, Zewen Wu, Yansong Tang, and Wenwu Zhu. Post-training quantization with progressive calibration and activation relaxing for text-to-image diffusion models. In *Proceedings of the European Conference on Computer Vision*, 2024. [2](#), [3](#)
- [56] Senmao Tian, Ming Lu, Jiaming Liu, Yandong Guo, Yurong Chen, and Shunli Zhang. CABM: Content-aware bit mapping for single image super-resolution network with large input. In *Proceedings of the IEEE/CVF Conference on Computer Vision and Pattern Recognition*, pages 1756–1765, 2023. [1](#), [3](#)
- [57] Mart Van Baalen, Christos Louizos, Markus Nagel, Rana Ali Amjad, Ying Wang, Tijmen Blankevoort, and Max Welling. Bayesian bits: Unifying quantization and pruning. In *Proceedings of the Advances in Neural Information Processing Systems*, pages 5741–5752, 2020. [5](#)
- [58] Jianyi Wang, Kelvin CK Chan, and Chen Change Loy. Exploring clip for assessing the look and feel of images. In *Proceedings of the AAAI Conference on Artificial Intelligence*, pages 2555–2563, 2023. [8](#)
- [59] Kuan Wang, Zhijian Liu, Yujun Lin, Ji Lin, and Song Han. HAQ: Hardware-aware automated quantization with mixed precision. In *Proceedings of the IEEE/CVF Conference on Computer Vision and Pattern Recognition*, pages 8612–8620, 2019. [1](#), [3](#)
- [60] Jiazheng Xu, Xiao Liu, Yuchen Wu, Yuxuan Tong, Qinkai Li, Ming Ding, Jie Tang, and Yuxiao Dong. ImageReward: Learning and evaluating human preferences for text-to-image generation. In *Proceedings of the Advances in Neural Information Processing Systems Workshop*, 2023. [1](#)
- [61] Chuanguang Yang, Zhulin An, Helong Zhou, Fuzhen Zhuang, Yongjun Xu, and Qian Zhang. Online knowledge distillation via mutual contrastive learning for visual recognition. *IEEE Transactions on Pattern Analysis and Machine Intelligence*, 45(8):10212–10227, 2023. [1](#)
- [62] Lvmin Zhang, Anyi Rao, and Maneesh Agrawala. Adding conditional control to text-to-image diffusion models. In *Proceedings of the IEEE/CVF International Conference on Computer Vision*, pages 3836–3847, 2023. [1](#)
- [63] Xuechen Zhang, Zheng Li, Samet Oymak, and Jiasi Chen. Text-to-3d generative ai on mobile devices: Measurements and optimizations. In *Proceedings of the Workshop on Emerging Multimedia Systems*, pages 8–14, 2023. [1](#)



# Text Embedding Knows How to Quantize Text-Guided Diffusion Models

## Supplementary Material

In this supplementary document, we present additional results and analyses, including the following:

- Results on a large-scale diffusion model (Section A).
- Evaluation on mixed-precision quantization method (Section B).
- Ablation studies on bit selection criteria (Section C).
- Ablation studies on bit precision options (Section D).
- Batch inference scenario analysis (Section E).
- Memory requirement analysis (Section F).
- Details on the structure and implementation of the T2Q module (Section G).
- Implementation details for ablation studies (Section H).
- Quantization sensitivity analysis for each layer (Section I).
- Additional visual comparison results.(Section J).

### A. Results on a Large-Scale Diffusion Model

We conducted experiments using SDXL [40] with the Euler scheduler as the base model to evaluate the effectiveness of QLIP on a large-scale diffusion model. As shown in Table S1, QLIP demonstrated significant improvements in computational efficiency while maintaining competitive image quality.

For the COCO2017 dataset, QLIP effectively reduced the computational complexity of the baseline diffusion quantization methods. Specifically, Q-diffusion+QLIP (W4A{8,16,32}) demonstrated a significant reduction in FAB while maintaining comparable FID and sFID scores to Q-diffusion (W4A16). This result indicates that QLIP optimizes the bit precision selection effectively, reducing computational overhead without compromising image quality. The results on the Conceptual Captions dataset exhibited similar trends to those observed with COCO2017. These results suggest that QLIP generalizes well to large-scale diffusion models.

### B. Evaluation on Mixed-Precision Method

We compared with PCR [54], a recent mixed-precision quantization method, using FLUX [1] as the base model. For image quality, we reported ImageReward [60] and PickScore [23], using 500 prompts from COCO2017. As shown in Table S2, applying our QLIP to PCR further improved performance by achieving higher quality scores while also reducing overall bit usage, demonstrating its effectiveness even on the recent diffusion model FLUX.

COCO2017				
Method	FAB $\downarrow$	FID $\downarrow$	sFID $\downarrow$	CLIP Score $\uparrow$
SDXL [40]	32.00	23.75	65.85	0.3180
Q-diffusion [27]	16.00	28.46	67.54	0.3178
+QLIP	12.68	28.16	66.31	0.3177

Conceptual Captions				
Method	FAB $\downarrow$	FID $\downarrow$	sFID $\downarrow$	CLIP Score $\uparrow$
SDXL [40]	32.00	19.25	47.72	0.3085
Q-diffusion [27]	16.00	22.23	49.57	0.3075
+QLIP	11.34	21.95	48.61	0.3074

Table S1. Quantitative comparisons at a resolution of  $768\times 768$  using SDXL [40]. For the bit precision options, W4A16 was used for Q-diffusion and W4A{8,16,32} were used for QLIP.

Method	FAB $\downarrow$	Image Reward $\uparrow$	Pick Score $\uparrow$
FLUX [1]	16.00	1.1013	23.07
PCR [54]	9.60	0.9986	22.97
+QLIP	7.92	1.0214	23.01

Table S2. Quantitative comparisons with the mixed-precision quantization method PCR, using FLUX as the baseline model. Evaluation was conducted on 500 prompts from the COCO2017 dataset at a resolution of  $1024\times 1024$ . For the bit precision options, W4A{8,16} was used for PCR, and W4A{6,8,16} were used for QLIP.

Bit Selection Strategy	FAB $\downarrow$	FID $\downarrow$
Image Complexity	14.86	31.09
Prompt Length	12.79	31.49
Image Quality (QLIP)	12.14	30.01

Table S3. Comparison of bit selection criteria.

### C. Ablation Studies on Bit Selection Criteria

We conducted experiments to explore alternative criteria for determining bit precision, replacing the predicted image quality used in our T2Q module. Specifically, we investigated two alternative metrics: image complexity and prompt length, as shown in Table S3.

Image complexity has been effectively used in other tasks, such as super-resolution, as a criterion for dynamic

Bit-Options	FAB $\downarrow$	FID $\downarrow$
{8,16}	10.51	24.78
{8,16,32}	10.58	24.72
{6,8,16,32}	9.24	25.22

Table S4. Ablation study on bit precision options for QLIP.

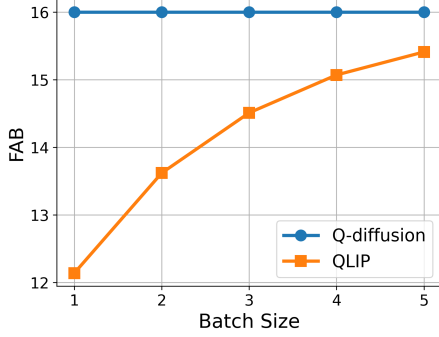


Figure S1. Bit allocation over different batch sizes.

Layer No.	Operator	Kernel ( $C_{in} \times C_{out}$ )
1	Linear / ReLU	$C_{clip} \times C_{clip}$
2	Linear / ReLU	$C_{clip} \times 512$
3	Linear / ReLU	$512 \times 1$
4	Sigmoid	-

Table S5. The structure of the T2Q module.

quantization [20]. To test its applicability in diffusion models, we replaced the T2Q and Q2B modules with T2C and C2B modules that utilize image complexity, measured as average image gradient magnitude. However, this configuration resulted in worse performance (FAB 14.86, FID 31.09) compared to the original QLIP design (FAB 12.14, FID 30.01), suggesting that image complexity alone is not a reliable criterion for bit selection in diffusion models.

We also evaluated a prompt length-based bit allocation strategy, where the number of tokens in the input prompt was used to decide bit precision. This variant also underperformed (FAB 12.79, FID 31.49) relative to our original approach. Unlike prompt length, which only reflects the input length, the T2Q module captures richer semantic representations from text, leading to more accurate bit assignment and better image quality.

## D. Ablation Studies on Bit-Options

The impact of different bit-options on FAB and FID is presented in Table S4. The results demonstrate that while the {6,8,16,32} configuration achieves the lowest FAB, it

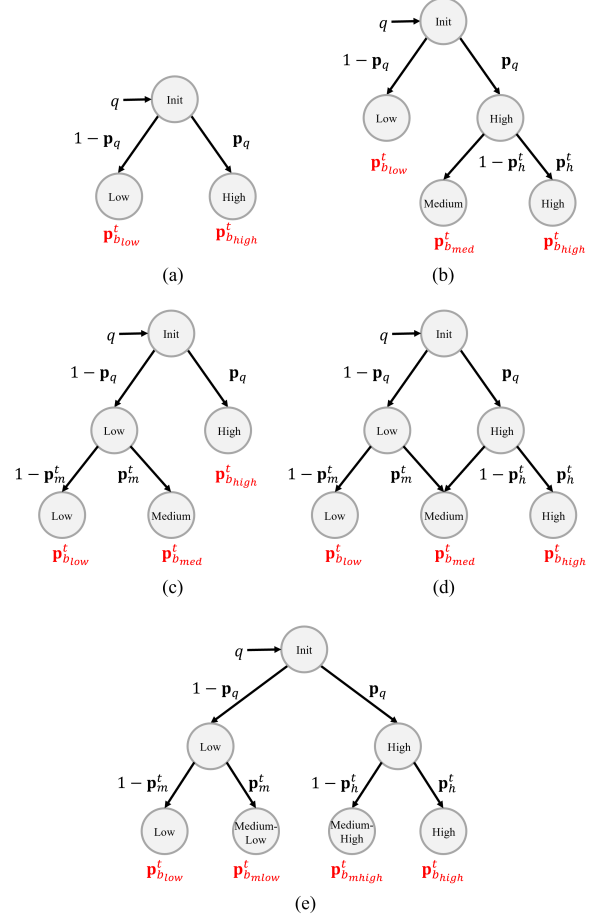


Figure S2. Implementation details of ablation study variants for the Q2B module. (a) Bit-Options correspond to the case with 2 bit candidates using  $p_q$ . (b), (c), and (d) correspond to the case with 3 bit candidates using  $p_q + p_h$ ,  $p_q + p_m$ , and  $p_q + p_m + p_h$ , respectively. (e) Bit-Options correspond to the case with 4 bit candidates.

also leads to an increase in FID. Conversely, the {8,16,32} configuration results in the lowest FID while maintaining a relatively low FAB, making it a better choice for minimizing image degradation and effectively reducing computational overhead. Based on these findings, we select {8,16,32} as the default bit-option.

## E. Batch Inference Scenario

Our practical implementation strategy for batch processing is to assign the maximum required bit precision for each layer across the batch. As shown in Fig. S1, the effectiveness of QLIP decreases as the batch size increases, which is a known limitation of input-adaptive quantization methods. However, text-to-image generation is typically performed on individual prompts or small batches. For exam-

ple, the recent GPT Image 1 API [2] provided by OpenAI officially supports small batch sizes per API call, and processing many images requires issuing multiple parallel API calls, rather than increasing the batch size within a single request. Therefore, this limitation has less significant practical impact.

## F. Memory Requirements

QLIP requires additional memory to store the model, including 1.5MB for the T2Q module and 12.1KB for the Q2B module, and additional 2.2KB for scale and zero-point values. However, this additional memory overhead is negligible compared to the total memory of BK-SDM-Tiny-2M 4bit (154.2MB). While our method does not reduce memory usage, it improves both energy efficiency and inference time by reducing the computational cost.

## G. Structure of the T2Q module

As shown in Table S5, the T2Q module consists of a simple 3-layer MLP with a ReLU activation function. The first linear layer is the projection layer of the CLIP text encoder, which is frozen during training. In the final layer, a sigmoid function is used to limit the output range of the quality  $q$ .

## H. Implementation Details on Ablation Studies

The implementation of the Q2B modules used in ablation studies is shown in Figure S2. When only  $\mathbf{p}_q$  is used,  $\mathbf{p}_{med}^t$  is not included, limiting the bit-options to two candidates. When  $\mathbf{p}_l^t$  (or  $\mathbf{p}_h^t$ ) is not used,  $\mathbf{p}_{low}^t$  (or  $\mathbf{p}_{high}^t$ ) is determined using  $\mathbf{p}_q$ , adjusting the available three-bit candidates accordingly. Incorporating additional bit-options, such as  $\mathbf{p}_{mlow}^t$  and  $\mathbf{p}_{mhigh}^t$ , can further increase the number of bit candidates.

## I. Analysis on Quantization Sensitivity

Figure S3 shows the proportion of bits used in each layer of the quantized denoising model. Stable Diffusion utilizes cross-attention blocks to incorporate text prompts into the image latent space, in addition to basic residual blocks. Notably, our proposed QLIP aims to manage the overall bit usage, particularly by assigning low bits more frequently on the layers in cross-attention blocks. Specifically, it is evident that bit reduction occurs mainly within three layers: (1) “proj\_in” which leverages the denoised image latent passed into the cross-attention block, (2) “at2.to.v” which projects text prompt to denoised image latent, (3) “proj\_out” which passes out the result of cross-attention to the next denoising blocks. These results are attributed to many cases with a weak correlation between the generated image and the text prompt, promoting the T2Q and Q2B modules to determine low bits for efficient quantization.

## J. Additional Qualitative Results

Figure S4 presents additional examples illustrating how changes in FAB are influenced by the richness and specificity of the text descriptions, along with the generated images. As shown, QLIP assigned higher bits when the text provides more specific and detailed descriptions, demonstrating that it leverages textual information to adapt bit precision, enabling effective synthesis of vivid details and textures.

Figures S5 and S6 show additional examples of the bit selection results and generated images using Q-diffusion or PTQD as baseline quantization methods. Figure S7 provides examples of images generated by QLIP using Q-diffusion or PTQD as baseline quantization methods, along with the full-precision model. The text prompts for generating images were sourced from the captions of COCO2017 and Conceptual Captions datasets.



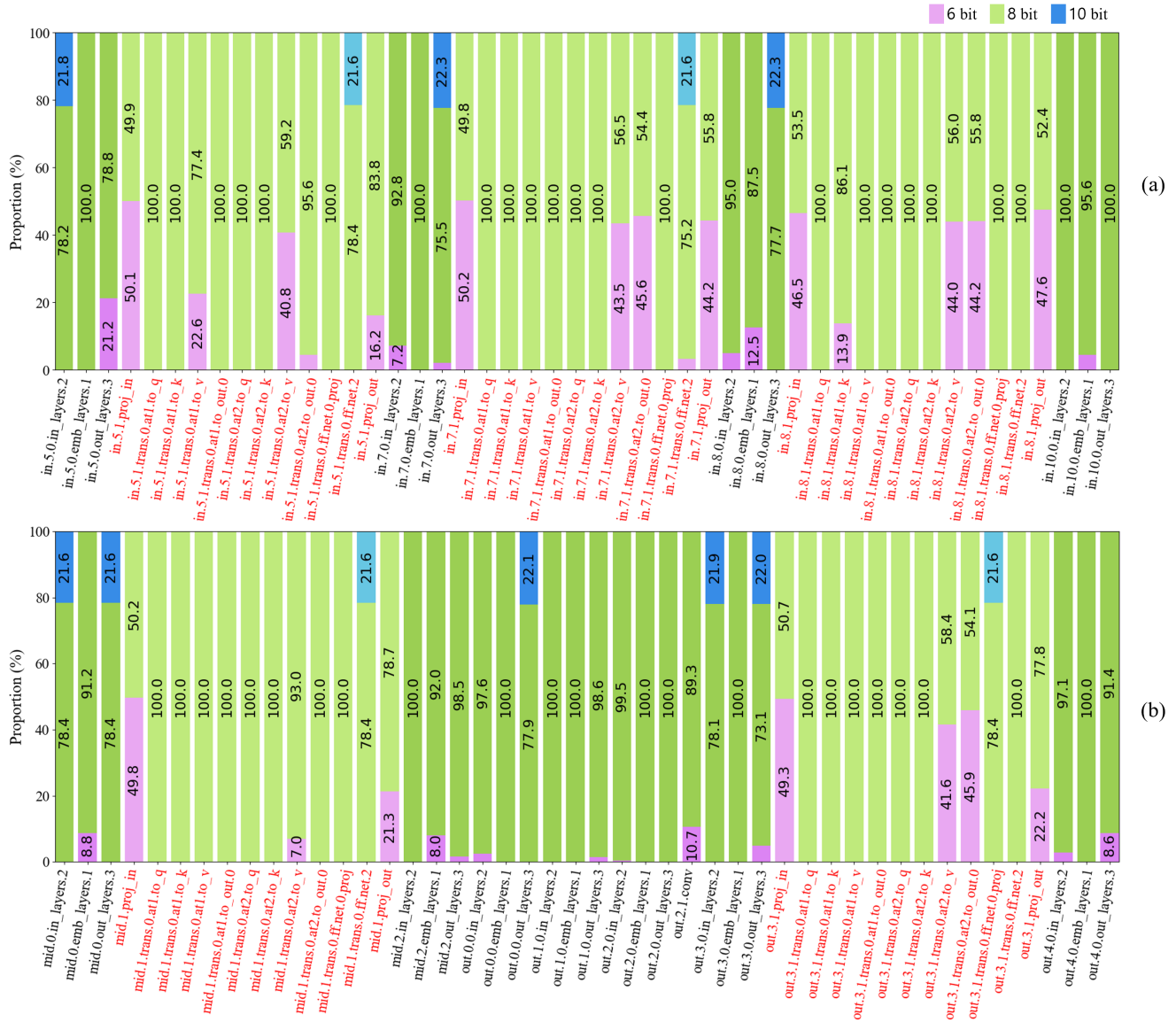


Figure S3. The proportion of bits assigned in each layer of the Stable Diffusion model quantized by W4A{6,8,10} using Q-diffusion w/ QLIP while generating 10k images using the COCO2017 validation dataset. On the x-axis, cross-attention blocks and residual blocks are indicated in red and black, respectively. (a) and (b) show the statistics of several layers in the input, middle and output blocks.






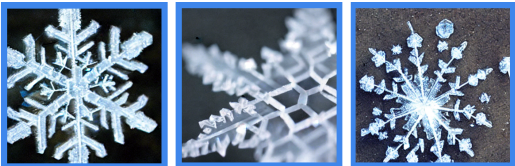

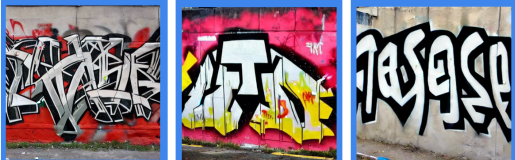
Images			Richness controlled captions	FAB
			volcano	14.30
			volcano erupted with a loud roar.	14.40
			volcano erupted with a loud roar, spewing lava.	14.48
			volcano erupted with a loud roar, spewing lava and ash.	14.51
			volcano erupted with a loud roar, spewing lava and ash into the sky.	14.97
			rainbow	14.54
			rainbow, a stunning natural phenomenon.	14.81
			rainbow, a stunning natural phenomenon, forms a bright, multicolored arc in the sky.	14.99
			rainbow, a stunning natural phenomenon, forms a bright, multicolored arc in the sky, displaying colors.	15.00
			rainbow, a stunning natural phenomenon, forms a bright, multicolored arc in the sky, displaying colors in the order of red, orange, yellow, green, blue, indigo, and violet.	15.12
			snowflake	14.04
			snowflake is a tiny intricate crystal of ice.	14.06
			snowflake is a tiny intricate crystal of ice with patterns.	14.10
			snowflake is a tiny intricate crystal of ice often shaped like a star with patterns.	14.28
			snowflake is a tiny intricate crystal of ice often shaped like a star with symmetrical patterns.	14.78
			spray painting	13.64
			spray painting creates bold, colorful images on walls.	13.83
			spray painting adds layers of bright, swirling graffiti on urban walls.	13.85
			spray painting can be made more descriptive by adding the following words: graffiti or street art	14.28
			spray painting can be made more descriptive by adding the words graffiti or street art to emphasize its appearance.	14.24

Figure S4. Examples of variations in FAB by QLIP for the texts with different levels of richness and detail, along with the generated images.

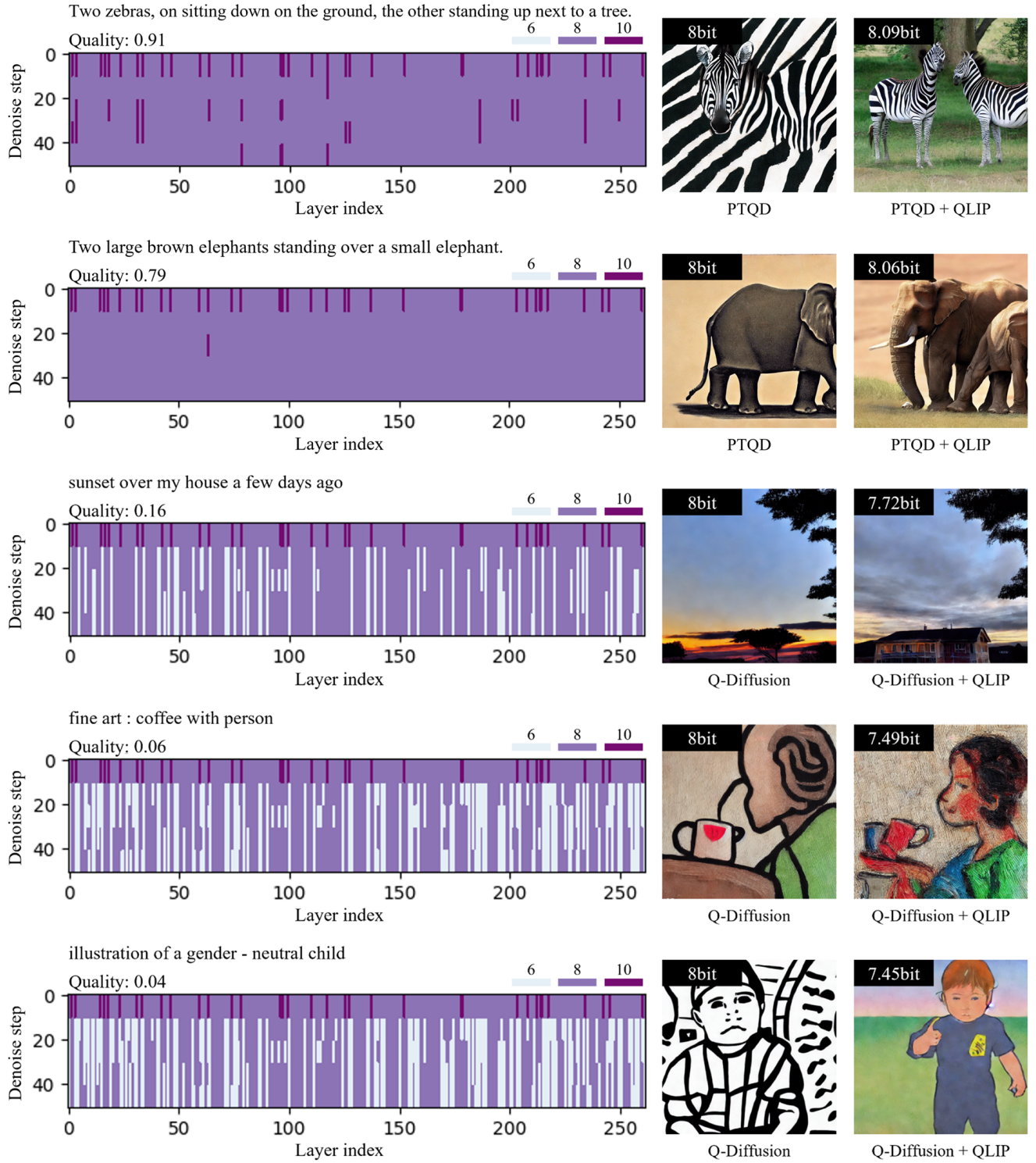


Figure S5. Examples of the bit selection results and generated images using Q-diffusion or PTQD as baseline quantization methods. QLIP is applied with the bit precisions of  $W4A\{6,8,10\}$ .



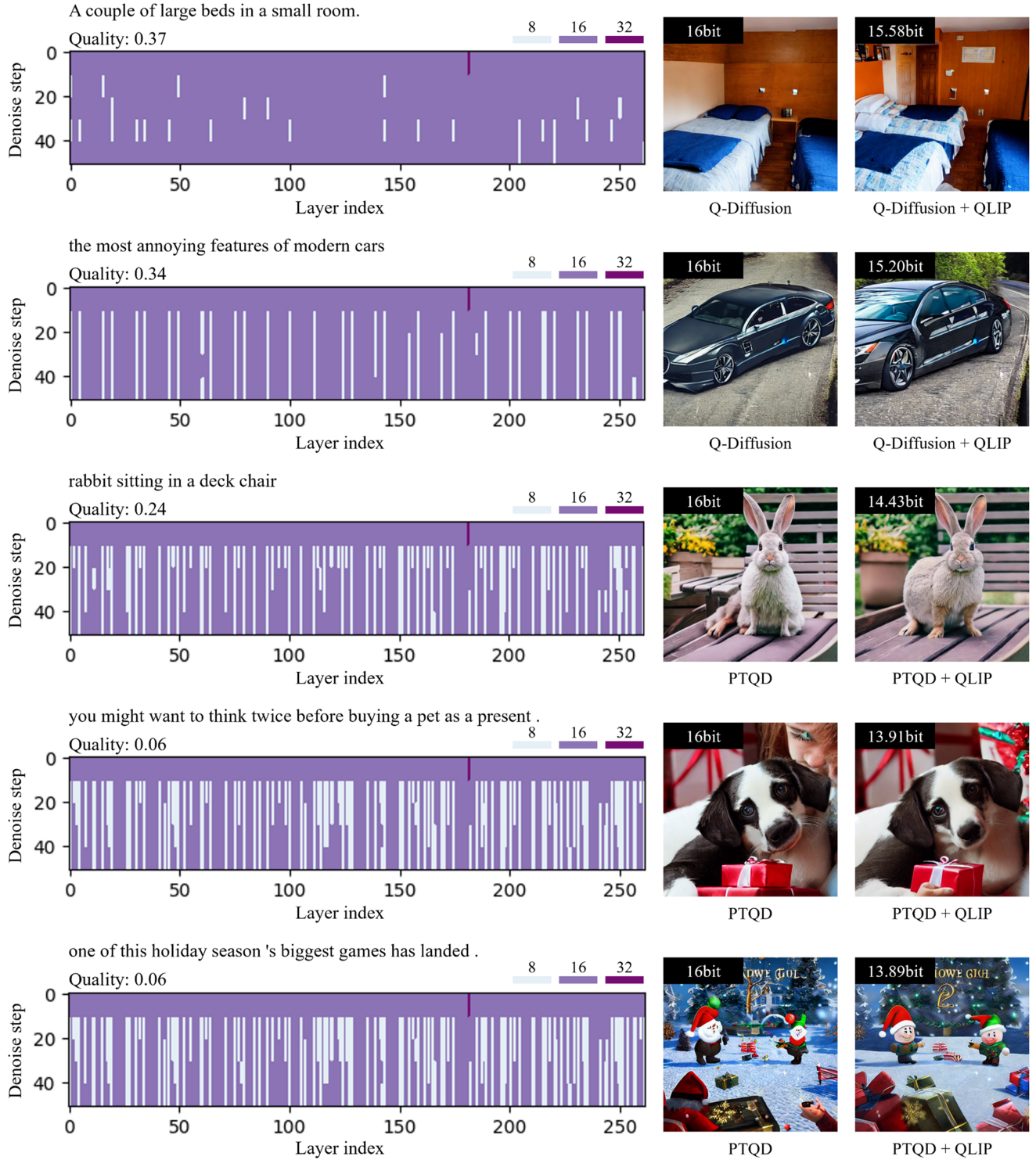


Figure S6. Examples of the bit selection results and generated images using Q-diffusion or PTQD as baseline quantization methods. QLIP is applied with the bit precisions of W4A{8,16,32}.



A large long train on a steel track.



A very tall church with a clock below a tower.



rainbow after a light shower .



a ferris wheel and wires in a cloudy sky



movement of water in the stones



Full precision

Q-diffusion

Q-diffusion + QLIP

PTQD

PTQD + QLIP

Figure S7. Examples of generated images using QLIP with Q-diffusion or PTQD as baseline quantization method.